Size-Dependent Electronic Structure Controls Activity for Ethanol Electro-Oxidation at Pt_n/Indium Tin Oxide (n = 1 to 14)

Alexander von Weber, Eric T. Baxter, Sebastian Proch, Matthew D. Kane, Michael Rosenfelder, Henry S. White, and Scott L. Anderson*

Department of Chemistry, University of Utah, 315 S. 1400 E., Salt Lake City, UT 84112

*anderson@chem.utah.edu

Supporting Information

Materials and Methods
Figures S1-S6
References (1-65)

STEM/HAADF Characterization of Pt_n deposited on carbon

As part of the acceptance testing of a new JEOL JEM 2800 scanning transmission electron microscope, we prepared lacey carbon TEM grids by depositing ~4 % of a ML of Pt in the form of Pt_1, Pt_7, or Pt_{14}. To allow this experiment, the normal sample holder used in preparation of the Pt_n/ITO samples, was replaced with a home-made mount that allowed several TEM grids to be clamped over holes in a backing plate. The grid mount was then positioned in front of the deposition beamline, and each grid was exposed to a beam of a different cluster size.

Deposition was done to a nominal coverage of 4% of a Pt monolayer (i.e., 40% of the coverage used in the electrochemistry work), however, several factors make the actual coverages on the grids uncertain, and probably cluster size-dependent. As usual, coverage was controlled by monitoring deposition current, however, in this case some fraction of the clusters would have passed through the open areas in the lacey carbon, and through the hole onto the backing plate, thus giving deposition current smaller than what would be observed on a solid substrate. As a result, the grids would tend to have had higher than 4% coverage. On the other hand, the clamp used to hold the TEM grids to the backing plate prevented getting the grids close to the deposition mask, and we know that our cluster beam tends to spread with distance from mask, due to space charge. To the extent that the cluster spot was larger than the 2 mm mask diameter, this would result in lower coverage on the grids. Because the space charge effect is higher for smaller clusters, the spreading effect is also size-dependent, and the actual coverage probably increased with increasing cluster size. As time was limited for these experiments, and the primary goal was to see if the new microscope would have sufficient contrast to image small clusters at all, we did not attempt to quantify the actual coverage.

The samples were imaged in STEM/ HAADF mode, with typical results shown in Fig. 2 of the manuscript. Selected area energy dispersive x-ray spectroscopy (EDS) was used to verify that the observed spots were, indeed, due to Pt.

There are several points of interest. The samples prepared with Pt_7 and Pt_{14} show obvious bright spots in the dark-field images, shown by EDS to be Pt, and it can be seen that the Pt_{14} spots are significantly brighter and appear somewhat larger than the Pt_7 spots. Given the uncertainty in the actual coverages, it is not possible to quantitatively compare the spot densities

to the expected coverages, however, the spot densities are certainly in the right range. For example, if the deposition density were exactly 4% of a ML, then the average spacing between Pt_{14} spots would be 4.8 nm, and the Pt_7 average spacing would be ~3.4 nm. Thus, the size and contrast of the spots and their spacings on the grids, are consistent with the deposited Pt_7 and Pt_{14} remaining intact, rather than breaking up or sintering on the carbon TEM grids.

The image for the grid prepared by Pt_1 deposition, in contrast, shows no obvious structure, and no structure was observed in a series of images taken with various magnifications and focusing conditions. It is not surprising that we were unable to image single Pt atoms using this non-aberration-corrected instrument, however, this result also provides important insight. As discussed in the main text, there are reasons to expect deposited atoms to diffuse and sinter more readily than deposited clusters. If, however, deposited atoms diffused efficiently under these conditions, then we would expect to have observed clusters formed by agglomeration. The conclusion is that at least for Pt_n on carbon under the conditions studied, there is no evidence of efficient agglomeration of either clusters or deposited atoms.

Pt 4d XPS

As described in the main text, XPS was used to characterize the Pt_n/ITO samples immediately after cluster deposition. A typical spectrum is shown in Figure S1, showing the two spin orbit components of the Pt 4d XPS feature, with interfering signal from argon implanted by sputtering. To avoid possible effects of the Ar 2s peak on the extracted Pt binding energies, the $4d_{3/2}$ peak was used.
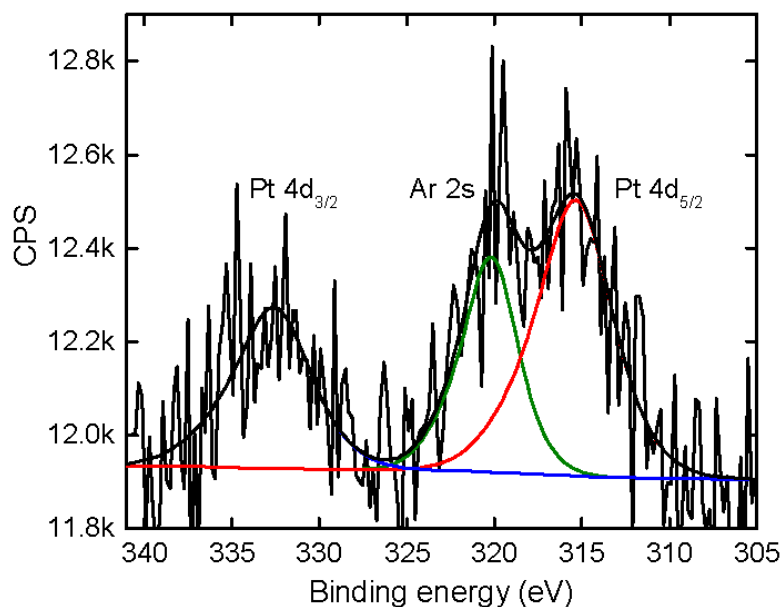
Fig. S1. A typical Pt 4d XP spectrum for Pt_n/ITO.

Initial scans on Pt_n/ITO electrodes

As described in the main text, each Pt_n/ITO electrode was initially probed by a series of CVs, all starting at the same lower limit potential, but scanning to increasing upper potential limits. An example of such a data set is shown in Figure S2.

Preparation of Control Electrodes

To provide context for the Pt_n/ITO results, three types of "control" electrodes were also studied: polycrystalline Pt ("Pt_{poly}"), Pt-free ITO, and ITO with Pt nanoparticles produced by solution deposition and reduction ("Pt_{nano}/ITO"). For the Pt-free ITO, the measurements were done using the same procedures described in the main manuscript, used in studied of the Pt_n/ITO electrodes. For the Pt_{poly} and Pt_{nano}/ITO electrodes, the measurements were made using a mock-up of the cell/antechamber arrangement used in the cluster experiments, but assembled on the bench top, and purged with N_2, rather than being evacuated.

The polycrystalline Pt electrode was prepared by mechanical polishing, ultrasonication in ethanol and water, two minutes etching in aqua regia (3:1:4 HCl:HNO_3:water), followed by rinsing in 18.2 $M\Omega \cdot cm$ DI water. The Pt_{nano} electrode was made by drop casting an ethanol solution of H_2PtCl_6 onto a clean ITO substrate, with concentration adjusted to give a Pt coverage of ~10 ML, i.e., ~100 times that in the size-selected Pt_n/ITO electrodes. The electrode was then annealed at 473 K in an H_2 flow, in order to reduce the Pt and allow nanoparticles to grow by agglomeration on the electrode surface.[13, 14] Several Pt_{nano}/ITO electrodes were made using this procedure, and one was characterized by scanning electron microscopy, giving a Pt particle size distribution peaked near 5 nm, with few particles having sizes greater than 10 nm, and roughly ~15 % of the surface covered by Pt. Because the Pt_{poly} and Pt_{nano}/ITO samples were exposed to air in the process of introduction to the cell, they were electrochemically cleaned by cycling between -0.2V and 1.4 V vs. Ag/AgCl at 10 V/sec. until stable CVs were observed, and then fresh electrolyte was introduced to study EOR chemistry.
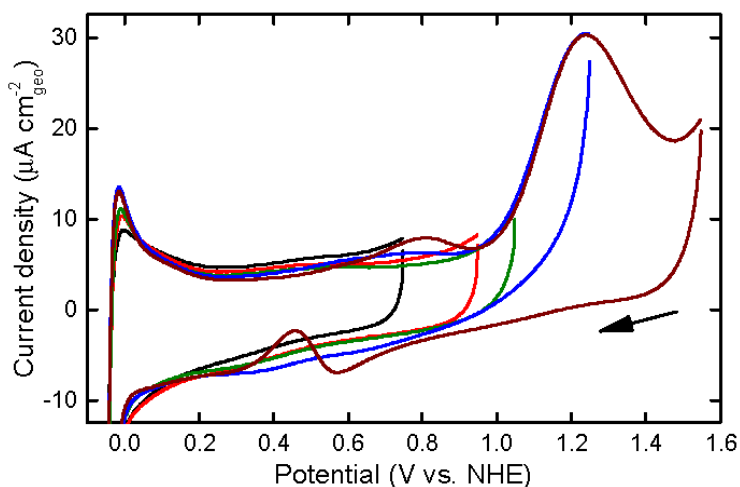
Fig. S2. Initial variable upper potential CV scans for Pt_{10}/ITO

Calculation of Current Densities.

The measured electrochemical currents are reported as current densities (A/cm^2), where the area used to normalize the currents is the geometric area of the active portion of the electrodes. For Pt_n/ITO, the active area is the cluster deposition spot, with nominal size of 0.031 cm^2, determined by the deposition mask. For most purposes here, the exact area of the cluster spot is unimportant, as long as it is smaller than the wetted area on the electrode, so that all the clusters are exposed to electrolyte. The wetted area was estimated by repeatedly sealing the cell to an ITO substrate, measuring the inside diameter of the O-ring contact by visualization through the transparent electrode, and also by SEM and optical visualization of marks/residues left on electrodes after electrochemical study. At minimum, the wetted area was ~0.04 cm^2, but if the force used to press the O-ring against the electrode was reduced, the wetted area could be up to 0.02 cm^2 larger. The only situation where the wetted area is important is in estimating the current densities for the Pt_{poly} and Pt_{nano}/ITO electrodes, where Pt is present over the entire surface. We have used 0.04 cm^2 for this purpose, thus the current densities for Pt_{poly} and Pt_{nano}/ITO are upper limits on the correct current densities.

For the Pt_n/ITO electrodes prepared by cluster deposition, we know the mass of Pt deposited quite precisely, thus it is trivial to use the measured currents to calculate the mass activities. These were obtained simply by dividing the peak, background-subtracted current at each EOR peak, by the amount of Pt deposited in the cluster spot (1.46 x 10-9 g for all but Pt_1, where half that coverage was used).

Related mass-selected electrochemistry work

Arenz, Heiz, and co-workers have used mass-selected cluster deposition to study the oxygen reduction reaction (ORR) over Pt_n deposited on carbon electrodes,[15] and demonstrated activity qualitatively similar to that seen for much larger supported Pt nanoparticles. The same group exploited cluster deposition to prepare catalysts where the cluster coverage could be varied, independent of the cluster size, and used this capability to explore cluster proximity effects on ORR.[16] They also combined cluster deposition, transmission electron microscopy, and electrochemistry to examine how deposited clusters migrate and evolve under electrochemical conditions.[17] Vajda and collaborators have developed a similar capability, and recently reported a study of OER at small Pd clusters deposited on diamond-coated electrodes, showing a strong increase in activity with deposited size.[18] They also applied X-ray scattering to characterize changes in the clusters, and theory to probe the nature of the reaction mechanism. Recently, they found striking effects of deposited Ag cluster size on the morphology of Li_2O_2 products formed from operating $Li-O_2$ batteries with size-selected Ag_n^+ deposited on the carbon cathode.[19]

The above experiments were done *ex situ*, i.e., the cluster-containing electrodes were removed from the deposition vacuum system, and exposed to air prior during transfer to the other tools used in the studies. This has the considerable advantage of allowing use of sophisticated analysis tools, but exposure of the clusters to adventitious adsorbates can modify the activity, as discussed in the main text and elsewhere.[1] Electrochemical cycling can be used to restore activity by removing the adsorbates, but it is unclear what other changes might occur during the cycling process.[17]

To avoid this complication, we developed an instrument to allow size-selected electrodes, prepared and characterized in UHV, to be transferred to the aqueous electrochemical environment without air exposure. We recently reported a study of ORR at Pt_n deposited on glassy carbon substrates without air exposure,[1] where we found that electrodes with certain

cluster sizes (e.g., Pt_7) showed activity similar to that seen for polycrystalline Pt or Pt nanoparticles supported on glassy carbon. Electrodes with other cluster sizes deposited (e.g. Pt_4, Pt_9) behaved very differently, catalyzing oxidation of the glassy carbon substrate by water with essentially no overpotential, and very fast kinetics. The factor that determined whether the Pt_n would act as ORR or carbon oxidation catalysts was the electronic structure of the clusters, as probed by X-ray photoelectron spectroscopy (XPS). Some experiments were done in which the Pt_n/glassy carbon electrodes were briefly exposed to air prior to introduction to the electrochemical cell, and it was found that activity for both ORR and carbon oxidation was suppressed, and we were unable to restore activity by potential cycling. A similar instrument has been developed by Zhou and co-workers, which has, to date, been applied to electro-oxidation of ethanol[20] and methanol[21] at model SnO_x-on-platinum electrocatalysts (not size-selected). A complementary approach, also avoiding air exposure, is to deposit clusters directly onto the surface of a UHV-compatible solid electrolyte, as has been done by Harbich and co-workers.[22]

Janata and co-workers have developed an alternative approach for production of size-selected electrodes via sequential deposition of metal atoms into a polyaniline matrix.[23] They used this approach to study alcohol oxidation catalyzed by Au_n and Au_nPd_1 clusters,[24-26] observing strong size effects and even-odd alternations in activity. The approach is related to an earlier dendrimer templating method developed by Crooks and co-workers,[27-30] but appears to give true atomic resolution for much smaller clusters. Such methods are critical for development practical size-selected catalysts, since they can produce catalyst at higher rates/lower costs.

Subtraction of non-EOR background current for Pt_n/ITO

For the 0.4 to 1.4 V potential range where the EOR peaks are observed, the main source of background current is ITO capacitive current, which is quite featureless (cf. Figure 3D, main text). We also expect small currents from oxidation and reduction of the deposited Pt, however, this process is non-catalytic, and the currents are limited by the small amount of Pt present. To provide a reference CV for subtraction of non-EOR currents expected for the Pt_n/ITO samples, we measured a CV for a separately prepared Pt_{10}/ITO sample, run in N_2-saturated 0.1 M $HClO_4$, without ethanol. As shown in Figure S3, the CV is dominated by capacitive current from the ITO support (cf. Figure 3D, main text), with superimposed peaks for the hydrogen evolution reaction (HER), H_2 oxidation, and small features for oxidation and reduction of the Pt_n. The onset of the oxygen evolution reaction (OER) can be seen above 1.5 V.

There are several important points:

1. The dominant contribution in the potential ranges of the EOR peaks is simply the ITO capacitive current. Given that all samples have the same low Pt coverage (0.1 ML), we do not expect this contribution to the background to depend significantly on Pt_n size.

2. The current for OER becomes significant only above ~1.5 V, i.e., well above the potential of the 2nd oxidation peak in EOR (1.2 – 1.25 eV), and, therefore does not contribute to the background current underlying this peak.

3. Similarly, the HER and H_2 oxidation signals are well below the potential range where the 1st oxidation and reactivation peaks are seen under EOR conditions, and therefore do not contribute to the background currents.

4. The integrated currents associated with Pt oxidation (0.9 < V < 1.4) and reduction (0.4 < V < 0.8) are small compared to the current from ITO, and because the amount of Pt deposited on each Pt_n/ITO sample is identical, it is reasonable to assume that variation in these small currents will be negligible compared to the EOR peak currents.
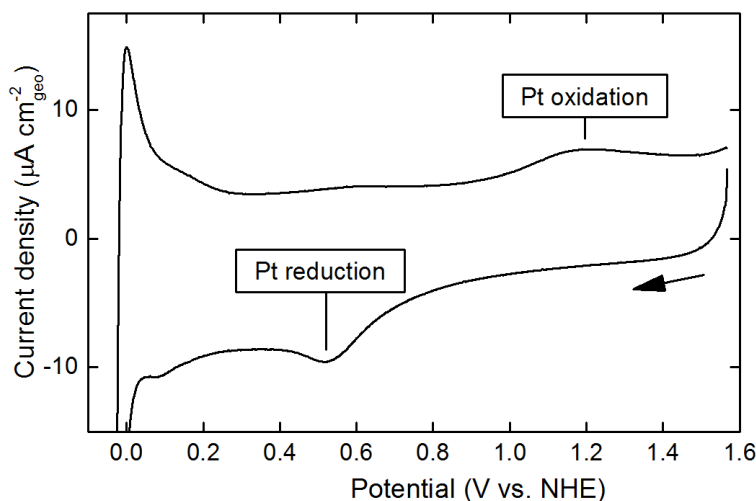
Fig. S3. CV of Pt_{10}/ITO in N_2-saturated $HClO_4$ without ethanol

Therefore the CV in Fig. S3 was used to estimate the subtraction of non-EOR background currents for all the Pt_n/ITO samples.

Comparison of Pt_n/ITO to control electrodes

It is useful to compare the currents seen for the Pt_n/ITO electrodes, with those for Pt_{nano}/ITO and Pt_{poly} electrodes. On a current per wetted area basis, as plotted in Figure 3, the Pt_{nano}/ITO peak currents average roughly 14% of those seen for Pt_{poly}, which is consistent with the estimation from SEM imaging that only ~15% of the surface of the Pt_{nano}/ITO electrode is Pt-covered. As discussed above, these current densities are upper limits, because they were calculated based on the minimum size of the wetted area. The Pt_n/ITO electrodes have 0.1 ML Pt coverage, thus if all Pt atoms were exposed on the surface, and have activity per atom similar to Pt in the Pt_{poly} surface, we might expect current densities for Pt_n/ITO roughly 10 times smaller than the upper limit current densities for Pt_{poly}. In fact, the ratio is more like 50, even for the largest EOR peak (2nd oxidation) for the most active sample (Pt_4/ITO). Part of the difference probably reflects the use of an upper limit for the Pt_{poly} current density.

From a practical perspective, it is more interesting to compare Pt_n/ITO and Pt_{nano}/ITO on the basis of Pt mass, i.e., EOR currents *per* gram Pt. For Pt_{nano}/ITO, the Pt loading was ~10 ML and the entire wetted area of the electrode contained Pt particles (~1.5 x 10^{16} Pt atoms/cm^2 on 0.04 cm^2 = ~1.9 x 10^{-7} g). The resulting peak currents *per* gram Pt (again, upper limits due to uncertainty in the wetted area) are ~46 A/g Pt, 72.5 A/g Pt, and 75 A/gm Pt, for the 1st oxidation, 2nd oxidation, and reactivation peaks, respectively. On a mass basis, the small clusters are generally quite active, as shown by comparison of these values with those shown in Figure 4. For the 1st oxidation peak, the most active Pt_n/ITO (Pt_4, Pt_{10}) have mass activities at least 4 times greater than that for Pt_{nano}/ITO, and aside from Pt_1/ITO which does not support the 1st oxidation peak, the Pt_n/ITO mass activities are at least equal to the upper limit measured for Pt_{nano}/ITO. Similarly, for the reactivation peak, Pt_4/ITO and Pt_{10}/ITO have mass activities that are ~8 and ~6 times, respectively, the upper limit value for Pt_{nano}/ITO, and the least active Pt_8/ITO sample as activity at least half that of the Pt_{nano}/ITO upper limit. For the 2nd oxidation peak, which is both the largest and the least dependent on cluster size, the mass activities for Pt_n/ITO range from >5 to ~15 times the upper limit Pt_{nano}/ITO activity.

The fact that the Pt_n/ITO electrodes have generally higher mass activities than Pt_{nano} is largely attributable to the expectation that most or all of the Pt atoms are in the surface layer for small Pt_n deposited on ITO. The fraction of Pt exposed in the surface layer for Pt_{nano}/ITO depends on particle size and morphology, and the fact that Pt_{nano}/ITO was prepared with 10 ML Pt coverage, yet had only part of the surface covered with nanoparticles, clearly shows that the particles were many layers thick, exposing only a small fraction of the Pt in the surface. Of course, such simple geometric considerations cannot explain why the activity for Pt_n/ITO varies so strongly and non-monotonically with cluster size.

Another point that is clear from comparing Pt_n/ITO and Pt_{nano}/ITO, is that the relative intensities of the three EOR peaks are quite different for Pt_n/ITO, compared to Pt_{nano}/ITO or Pt_{poly}. For Pt_{poly} the 1st oxidation, 2nd oxidation, and reactivation peaks have peak current densities in a 1 : 1.9 : 2.2 ratio, while for Pt_{nano}/ITO the ratio is similar (1 : 1.6 : 1.6). For Pt_1, the ratio is roughly 0 : 4 : 1, while for the other Pt_n, the ratio ranges from about 1 : 7.5 : 0.9 for the least active Pt_n/ITO (n = 7, 8), to 1 : 5 : 3.6 for the more active sizes like Pt_4 and Pt_{10}. In all cases, the 2nd oxidation peak is substantially stronger compared to the 1st oxidation or reactivation peaks, than it is for Pt_{poly} or Pt_{nano}/ITO.

Although the primary focus of the analysis has been on variations in the magnitudes of the EOR peaks, it is important to note that the potentials where the peaks currents are observed are lower than for Pt_{poly} or Pt_{nano}/ITO. For example, the 1st oxidation feature peaks at 0.89 V and 0.92 V for Pt_{poly}, and Pt_{nano}/ITO, respectively, while on Pt_n/ITO, the analogous feature peaks between 0.82 and 0.84, depending on cluster size. Similarly, the 2nd oxidation feature peaks at 1.3 V for Pt_{poly} and at 1.34 V for Pt_{nano}/ITO, but for Pt_n/ITO the peak current is observed between 1.24 V and 1.28 V. Finally, the reactivation feature peaks quite sharply at 0.64 V for both Pt_{poly} and at Pt_{nano}, but the much broader reactivation features for Pt_n/ITO peak in the range between 0.45 and 0.49. While these shifts are not large, and would have only a small effect on efficiency of a direct ethanol fuel cell, they are further evidence that the EOR kinetics are significantly different on small clusters, compared to bulk Pt or large Pt nanoparticles.

The CV cycle dependence of EOR activity.
Figure S4 shows two additional examples of the changes induced by potential cycling on the background-subtracted EOR peak current densities. Figure S4A shows results for Pt_1/ITO (at 0.1 ML coverage), and Fig. S4B shows results for a second Pt_4/ITO sample. As in Fig. 6, repeated CV cycling was found to result in several types of changes in the EOR activity over the course of each sequence of CVs. Early on during the cycling (first ~dozen CVs), the intensity of the reactivation peak increased rapidly, while the intensities of the 2nd oxidation peak, and in some cases, the 1st oxidation peak, decreased. For CVs collected during next 10-25 scans, the peak current densities continued to evolve, but at a slower rate. For most samples, the reactivation peak continued to increase slowly, with concurrent decrease in the 2nd oxidation peak. For one Pt_4/ITO sample, the reactivation peak also started to decrease slowly after ~13 CVs. In all cases, the peak current densities continued to evolve slowly for the next 15 – 30 CVs. Finally, the in the final stage of the sequences, there was rapid decline in EOR intensity to baseline over ~10 scans, and then followed by a long period of essentially zero EOR currents. As shown below, the final, rapid decrease to zero resulted from poisoning of the Pt_n by Cl⁻ diffusing from the reference electrode compartment. Possible mechanisms for the slower changes peak currents observed earlier in the CV sequences are discussed below.
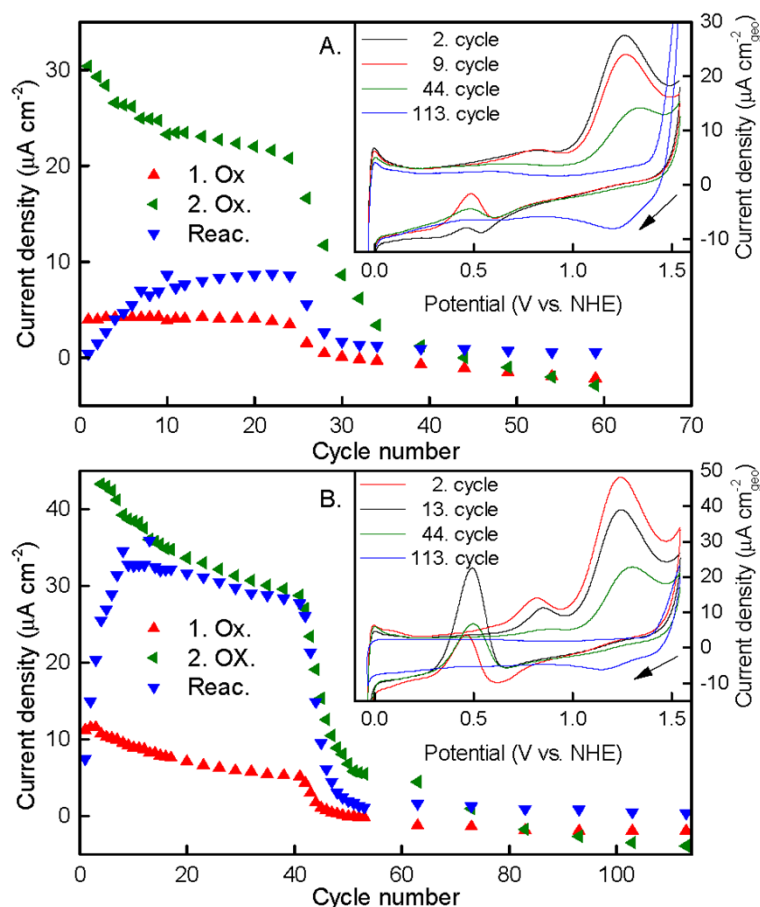
Fig. S4. Top: CV cycle dependence for Pt_1/ITO.   Bottom: CV cycle dependence for a second Pt_4/ITO sample.

Cluster size dependence at the beginning of the CV sequence for each sample.

One of the interesting results from this study is the strong oscillations of EOR peak currents cluster size, and the fact that these oscillations are anticorrelated with oscillations in the Pt core level binding energy measured by XPS (Figure 7, main text). To verify that the oscillatory behavior shown in Fig. 7 is not simply an artifact of having chosen to analyze currents in the CVs measured just at the end of the initial ~10 CV period of rapid change, Fig. S5 shows the analogous results based on the 2nd CV for each sample. It can be seen that the oscillatory size dependence is identical to that recorded later in the CV sequences. The only exception is that the reactivation peak is so weak at the beginning of the CV sequence that it is not possible to extract its background-subtracted intensity with any confidence. We conclude that the oscillatory structure is due to inherent, size-dependent properties of the ITO-supported Pt_n, and that the size distribution must not evolve significantly under potential cycling, at least for the first dozen cycles.
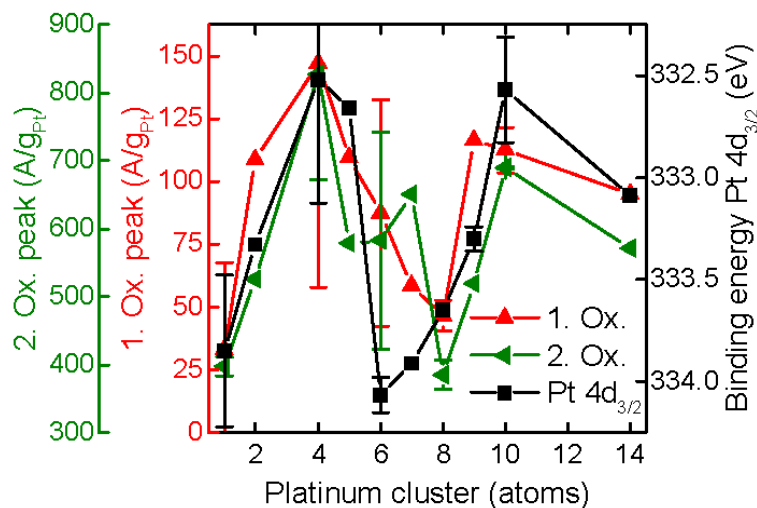
Figure S5. Cluster size dependence of the background-subtracted EOR peak currents taken from the 2nd CV on each sample.

Factors possibly contributing to changes in EOR currents.

In the early and middle stages of the CV sequences shown in Figs. 6 and S4, the relative intensities of the three EOR peaks change. Given the conclusion that the cluster size distribution is not evolving significantly, there are several possible factors that might cause the EOR peak currents to evolve.

One obvious question is whether consumption of the ethanol reactant is significant. It is not possible to quantitatively relate the integrated (background-subtracted) EOR currents to the amount of ethanol consumed, because we do not know what distribution of products is formed, and therefore how many electrons are required *per* ethanol molecule. The integrated EOR currents obviously depend on cluster size, but for Pt_4, the most reactive size, the integrated currents for all three EOR peaks amounted to ~1.95 x 10^{-6} C per cycle during the initial CVs. If we assume a product distribution similar to that measured by Wang et al.,[11] then ~4.12 electrons are generated *per* ethanol molecule consumed, thus we can estimate that about 5x10^{-12} moles of ethanol are consumed *per* cycle. The ethanol consumption is, therefore, negligible compared to the ~1.7x10^{-5} moles of ethanol initially present in the working compartment, although the ethanol concentration in the electrolyte layer near the electrode may become somewhat depleted.

Other factors that may change during potential cycling include cluster properties which may evolve due to cycling through the Pt oxidation/reduction potential, and changes in concentrations of reaction intermediates and products in the electrolyte and adsorbed on the Pt_n, modifying the relative rates of the reactions that give rise to the three peaks. Regardless of the cause of the current changes, the fact that the cluster size dependence remains sharp during potential cycling rules out significant broadening of the cluster size distribution.

The rapid decline in EOR signals after 25 – 30 CVs could potentially be due to build-up of EOR products (e.g. acetate) in the electrolyte, poisoning the surface.[36] To test this possibility, some CV sequences were stopped after the rapid EOR activity decay, to allow injection of fresh electrolyte into both the working and counter electrode compartments. In no case was significant recovery of EOR activity observed, indicating that the loss of activity resulted from changes in the Pt_n/ITO electrodes, not the electrolyte.

One such change might be dissolution of the Pt_n clusters, due to cycling of the potential through the Pt redox potential. Ideally, post-reaction Pt XPS could be used to directly measure Pt remaining on the electrodes, but a previous attempt[1] at such measurements yielded ambiguous results. The problem was that we were unable to rinse away all traces of electrolyte from the post-reaction electrode surfaces, thus it was not clear if post-reaction reduction in Pt XPS intensity was due to Pt loss by dissolution, or simply attenuation by an adsorbate overlayer.

Fortunately, the CVs, themselves, provide evidence that a significant fraction of the initial Pt remained on the ITO surface even after the EOR signal completely decayed. Figure 3D shows that Pt-free ITO does not catalyze HER in the potential range probed in our experiment, however, HER (and H_2 oxidation) are clearly present in the CVs taken after the EOR signal had completely decayed (Figures 6 and S4), showing that the electrodes continued to have significant Pt coverage, and that the Pt remained accessible to water, but apparently not to ethanol.

Cl⁻ is responsible for the final, rapid decline in EOR activity

All the CV sequences terminate in a rapid decline in EOR peak intensities, after which, the CVs shown no evidence of structure due to EOR. We attribute this decline to poisoning of the Pt_n/ITO by Cl⁻, which is known to bind strongly to Pt,[37, 38] and is present in the reference compartment with only a single frit slowing diffusion to the Pt_n/ITO electrode. To test this hypothesis, we conducted an experiment with a Pt_{poly} electrode, where the frit separating the reference and working compartments was replaced by a short piece of capillary tubing, in order to speed the diffusion between the compartments. As shown in Fig. S6, the decay in EOR peak intensity occurred over only ~5 CVs, concomitant with growth of a strong reduction feature at ~1.34 V in agreement with the expected potential for the reaction $Cl_2 + 2\ e^- \rightarrow 2Cl^-$ (E^o = 1.36 V vs. NHE). The Cl_2 is generated by the reverse reaction, to which we attribute the growth of a strong oxidation feature at potentials above ~1.4 V. Similar, but weaker reduction and oxidation features are observed in the final CVs on all the Pt_n/ITO samples (insets to Figs. 5 and S4). In the normal experimental configuration, where the cell compartments were separated by frits, the Cl⁻ poisoning effect was not seen during 120 CVs for Pt_{poly}, however, this is not unexpected. It took 25 to 40 CVs for Cl⁻ poisoning to become obvious for Pt_n/ITO, and Pt_{poly} has an order of magnitude more Pt surface sites, thus more Cl⁻ diffusion must occur before poisoning becomes obvious.
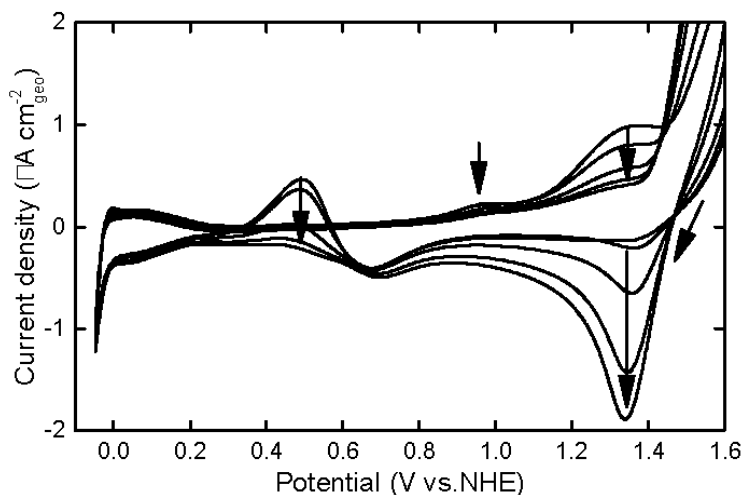
Figure S6. CVs for Pt_{poly} in 0.1 M $HClO_4$ with 1% Ethanol, where diffusion of Cl^- from the reference electrode was enhanced by replacing the normal frit with a short section of capillary tubing.

Cl^- contamination also explains why the rapid decline of EOR activity occurs after different numbers of CVs for different samples. Electrolyte injection into the cell was done by hand, and small variations in the amount of NaCl injected into the reference compartment were unavoidable. As a result, we expect that the extent of initial Cl^- permeation of the frit, and therefore the time required for significant Cl^- contamination to reach the working electrode would vary from day to day. One interesting question is whether the poisoning effect is simply a matter of site blocking, or if strong binding of electronegative Cl to the small Pt clusters changes the Pt electronic structure, reducing activity. The anti-correlation of Pt 4d BEs with activity suggests that activity requires electron-rich Pt sites, thus even a modest electron-withdrawing effect might be sufficient to inhibit EOR. The fact that HER and chlorine oxidation and reduction continue to be observed after EOR activity has completely decayed, suggests that Pt sites are still accessible, at least to small molecules.

Interpretation of XPS binding energies (BEs)

Core level BEs are influenced by a number of factors, which are often loosely described in terms of effects on the initial or final states of the photoemission process. The initial state is a Pt atom forming part of a Pt cluster, and its energy is influenced by the electron density in the local environment. The final state is the Pt atom with an electron missing from the 4d core orbital. The final state energy is stabilized by relaxation of other electrons in that atom, and by screening/delocalization of the core hole charge by flow or polarization of electrons in the surroundings.

The effects of particle size on XPS shifts have been studied for many metal/oxide systems. For example, gold films grown on SiO_2 and TiO_2 typically show bulk-like XPS BEs for thick films, but as the film thickness drops below ~2 ML and the average size of the particles present becomes small, the BE increases by up to 1.6 eV.[39, 40] Because gold is expected to remain in the Au^0 oxidation state, these shifts are primarily attributed to final state effects. The idea is that as particle size is reduced, screening of the core hole is less efficient because charge can only delocalize over the particle surface. The less stable final state results in BEs that increase with decreasing particle radius as $radius^{-1}$.[41, 42] On top of this smooth variation with size, there

may also be size-to-size oscillations in BEs that indicate size-dependent changes in the electronic properties of the supported clusters. For example, size-selected Pd_n/TiO_2,[43] Pd_n/alumina,[44] and Pt_n/glassy carbon,[1] all show an overall trend of decreasing BEs with increasing cluster size, superimposed on size-to-size fluctuations.

For comparison to the BEs for Pt_n/ITO, we measured the Pt $4d_{3/2}$ BE for polycrystalline Pt, and obtained a value of 331.8 eV, in good agreement with literature values.[45, 46] The BEs seen for Pt_n/ITO (Figure 7) average about 1.5 eV higher than this bulk limit, with fluctuations of up to ~1.5 eV, and no obvious sign that the BEs are converging toward the bulk limit, at least in this small size range.

Consider examples like Pt_4/ITO or Pt_{10}/ITO, which have lower-than-average Pt 4d BEs and high activity. From an initial state perspective, lower-than-average BE would suggest that the Pt is relatively electron rich, compared to other cluster sizes on ITO. From a final state perspective, low BEs would be rationalized in terms of efficient screening of the core hole by valence electrons, and screening would tend to be enhanced by the Pt_n valence levels being electron rich and/or highly polarizable. Thus from either initial or final state perspectives, Pt_n with low 4d BEs are seen to be electron rich, and it is these clusters that have high EOR activity.

Conversely, Pt_1/ITO, Pt_7/ITO and Pt_8/ITO have unusually high Pt 4d BEs and low EOR activity. An initial state picture would suggest that interaction of Pt with the ITO has resulted in relatively electron-poor Pt_n, while a final state picture would suggest poor screening of the core hole, consistent with fewer and/or less polarizable valence electrons on the Pt. From either perspective, these relatively inactive cluster sizes are seen to be depleted of easily polarized valence electrons. From a catalytic perspective, it appears that a high activity requires a high density (or high polarizability) of valence electrons on the Pt clusters.

Size dependent properties for free and supported Pt clusters

One question is whether the size-dependent properties of Pt_n/ITO reflect inherent properties of Pt_n, i.e., do they correlate with properties for Pt_n in the gas phase. There have been a number of experimental and theoretical studies of gas-phase Pt clusters providing information such as the stabilities,[47-49] orbital energies,[50] ionization energies,[51] and electron affinities.[51-54] These results show variations in properties with size, but there is no obvious connection to the pattern observed here for EOR activity. The exception is a theoretical finding[51] suggesting that Pt_4 is a local minimum in both ionization energy and electron affinity, however, in the case of electron affinity, where experiments exist, this theoretical finding is not borne out. Trends in gas-phase reactivity vs. cluster size are also interesting. The reactions studied most extensively are those with CH_4 and N_2O, and these provide some indications that gas-phase Pt_4 and Pt_{10} may be special under certain conditions. For example, CH_4 reaction with Pt_n in the cationic, neutral, and anionic states has been studied. For cations, Pt_4^+ and Pt_{10}^+ are found to have unusually *low* reaction efficiencies, suggesting that they may have particularly stable electronic structure.[55-57] The anions are generally less reactive than the cations, but there is no clear pattern in the size effects.[55-57] For neutral Pt_n, reaction with CH_4 is relatively efficient for n = 2-5, and the activity for the larger Pt_n is >4 times lower, with a local minimum at Pt_{10}.[48] Perhaps more germane to oxidation catalysis, reactions of oxidizers with Pt_n show similar effects. Pt_4^+ and Pt_{10}^+ are unusually unreactive with N_2O, while the anions show weaker size dependence, with particularly low activity for Pt_6^- and Pt_{10}^-.[58] Pt_4^- is also found to be more reactive with O_2 than neighboring sizes.[59] In reaction of N_2O with neutral Pt_n (n=4-12), Pt_4 is least reactive, but otherwise there is little effect of cluster size.[60] The most obvious conclusions to be drawn from these results are:

1. There are inherent size-dependence variations in Pt_n electronic properties which can affect reactivity. These do not directly correlate with what is observed for Pt_n/ITO, however, they suggest that interaction of deposited Pt_n with ITO is likely to be dependent on cluster size.

2. Reactivity is quite sensitive to charge state, which ties in with our observation that electron-rich (poor) Pt_n/ITO are particularly active (inactive).

The effects of Pt-support interaction on the electronic structure and catalytic activity can also be assessed by comparison with other Pt_n/support systems. The large (1.5 eV) BE fluctuations and lack of convergence toward the bulk limit seen for Pt_n/ITO are quite different from what is observed for Pt_n/alumina and Pt_n/glassy carbon. For Pt_n/glassy carbon[1] the fluctuations in the Pt 4f BE with size are only ~0.3 - 0.4 eV, and appear to converge toward the bulk with increasing size – the BE shifts relative to bulk Pt fall from ~0.7 eV for Pt_1 to ~0.2 eV for Pt_{11}. Another indication that the cluster-support interaction has a strong effect on the electronic properties is that fluctuations in BEs with size are quite different for Pt_n/ITO and Pt_n/glassy carbon. For Pt_n/glassy carbon, the sizes with higher-than-expected BEs were Pt_7, Pt_{10}, and Pt_{11}, compared to Pt_1, Pt_6, Pt_7, and Pt_8 for Pt/ITO. For Pt_n/alumina,[7] it was not possible to measure XPS BEs due to interference from the Re(0001) substrate underlying the alumina film, however, the onset of the Pt valence band was observed to converge from ~0.7 eV below the Fermi level (E_F) for Pt_2 to ~0.3 eV below E_F for Pt_{10}, with more gradual convergence between Pt_{10} and Pt_{18}. The fluctuations with cluster size were within the uncertainty (<0.1 eV). The larger shifts and stronger fluctuations seen for Pt_n/ITO suggest that there are strong size-dependent interactions with ITO that overwhelm the convergence expected from final state considerations.

In both Pt_n/alumina and Pt_n/glassy carbon, the variations in Pt binding energies were anti-correlated with activity for oxidation reactions. For Pt_n/alumina, CO oxidation was studied under UHV conditions, and CO_2 production was found to be anticorrelated with the Pt BEs, and positively correlated with the density of binding sites on top of the clusters. Similar anti-correlations have been observed for CO oxidation over several Pd_n/oxide systems,[43, 44, 61, 62]

References
1.	Proch, S.; Wirth, M.; White, H. S.; Anderson, S. L. *J. Am. Chem. Soc.* **2013,** 135, 3073−3086.
2.	Boyd, K. J.; Lapicki, A.; Aizawa, M.; Anderson, S. L. *Review of Scientific Instruments* **1998,** 69, 4106-4115.
3.	Thomas, J. M. *J. Chem. Ed.* **1999,** 76, 97-98.
4.	Rudy, B.; Iverson, L. E., *Ion Channels - Reprint of Volume 207 in Methods in Enzymology Series*. Acad. Pr.: New York, 1997.
5.	Qiu, H.; Yan, J.; Sun, X.; Liu, J.; Cao, W.; Yang, X.; Wang, E. *Anal. Chem.* **2003,** 75, 5435–5440.
6.	Klett, J.; Krähling, S.; Elger, B.; Schäfer, R.; Kaiser, B.; Jaegermann, W. *Z. Phys. Chem.* **2014,** 228, 503−520.
7.	Roberts, F. S.; Kane, M. D.; Baxter, E. T.; Anderson, S. L. *Physical chemistry chemical physics : PCCP* **2014,** Advance Article.
8.	Frumkin, A. N.; Aikazyan, E. A. *Bulletin of the Academy of Sciences of the USSR, Division of chemical science.* **1959,** 8, 188-197.
9.	Vigler, F.; Coutanceau, C.; Hahn, F.; Belgsir, E. M.; Lamy, C. *J. Electroanal. Chem.* **2004,** 563, 81-89.
10.	Leung, L.-W. H.; Chang, S.-C.; Weaver, M. J. *J. Electroanal. Chem.* **1989,** 266, 317-336.
11.	Wang, H.; Jusys, Z.; Behm, R. J. *Journal of Physical Chemistry B* **2004,** 108, 19413-19424.
12.	Giz, M. J.; Camara, G. A. *J. Electroanal. Chem.* **2009,** 652, 117-122.

13.   Schweizer, A. E.; Kerr, G. T. *Inorg. Chem.* **1978,** 17, 2326–2327.

14.   Vigier, F.; Coutanceau, C.; Perrard, A.; Belgsir, E. M.; Lamy, C. *Journal of Applied Electrochemistry* **2004,** 34, 439–446.

15.   Kunz, S.; Hartl, K.; Nesselberger, M.; Schweinberger, F. F.; Kwon, G.; Hanzlik, M.; Mayrhofer, K. J. J.; Heiz, U.; Arenz, M. *Phys. Chem. Chem. Phys.* **2010,** 12, (35), 10288-10291.

16.   Nesselberger, M.; Roefzaad, M.; Faycal Hamou, R.; Ulrich Biedermann, P.; Schweinberger, F. F.; Kunz, S.; Schloegl, K.; Wiberg, G. K. H.; Ashton, S.; Heiz, U.; Mayrhofer, K. J. J.; Arenz, M. *Nat. Mater.* **2013,** 12, 919-924.

17.   Hartl, K.; Nesselberger, M.; Mayrhofer, K. J. J.; Kunz, S.; Schweinberger, F. F.; Kwon, G. H.; Hanzlik, M.; Heiz, U.; Arenz, M. *Electrochimica Acta* **2010,** 56, (2), 810-816.

18.   Kwon, G.; Ferguson, G. A.; Heard, C. J.; Tyo, E. C.; Yin, C.; DeBartolo, J.; Seifert, S.; Winans, R. E.; Kropf, A. J.; Greeley, J.; Johnston, R. L.; Curtiss, L. A.; Pellin, M. J.; Vajda, S. *ACS Nano* **2013,** 7, 5808-5817.

19.   Lu, J.; Cheng, L.; Lau, K. C.; Tyo, E.; Luo, X.; Wen, J.; Miller, D.; Assary, R. S.; Wang, H.-H.; Redfern, P.; Wu, H.; Park, J.-B.; Sun, Y.-K.; Vajda, S.; Amine, K.; Curtiss, L. A. *Nat. Commun.* **2014,** 5, 4895 (8 pages).

20.   Zhou, W.-P.; Axnanda, S.; White, M. G.; Adzic, R. R.; Hrbek, J. *J. Phys. Chem. C* **2011,** 115, (33), 16467-16473.

21.   Zhou, W.-P.; An, W.; Su, D.; Palomino, R.; Liu, P.; White, M. G.; Adzic, R. R. *Journal of Physical Chemistry Letters* **2012,** 3, (22), 3286-3290.

22.   Falgairette, C.; Xia, C.; Li, Y.; Harbich, W.; Comninellis, C. *Journal of Applied Electrochemistry* **2010,** 40, (10), 1893-1900.

23.   Jonke, A. P.; Josowicz, M.; Janata, J. *Journal of the Electrochemical Society* **2011,** 158, (12), E147-E151.

24.   Jonke, A. P.; Josowicz, M.; Janata, J. *Journal of the Electrochemical Society* **2012,** 159, (3), P40-P43.

25.   Schwartz, I. T.; Jonke, A. P.; Josowicz, M.; Janata, J. *Catalysis Letters* **2013,** 143, (8), 777-782.

26.   Schwartz, I. T.; Jonke, A. P.; Josowicz, M.; Janata, J. *Catalysis Letters* **2013,** 143, (7), 636-641.

27.   Iyyamperumal, R.; Zhang, L.; Henkelman, G.; Crooks, R. M. *Journal of the American Chemical Society* **2013,** 135, (15), 5521-5524.

28.   Ye, H.; Crooks, J. A.; Crooks, R. M. *Langmuir* **2007,** 23, (23), 11901-11906.

29.   Ye, H.; Crooks, R. M. *Journal of the American Chemical Society* **2005,** 127, (13), 4930-4934.

30.   Zhao, M.; Crooks, R. M. *Advanced Materials (Weinheim, Germany)* **1999,** 11, (3), 217-220.

31.   Savinova, D. V.; Molodkina, E. B.; Danilov, A. I.; Polukarov, Y. M. *Rus. J. Electrochem.* **2004,** 40, 683-687.

32.   Gomes, J. F.; Bergamaski, K.; Pinto, M. F. S.; Miranda, P. B. *Journal of Catalysis* **2013,** 302, 67-82.

33.   Casella, I. G.; Desimoni, E. *Electroanalysis* **1996,** 8, 447-453.

34.   Rightmire, R. A.; Rowland, R. L.; Boos, D. L.; Beal, D. L. *J. Electrochem. Soc.* **1964,** 111, 242-247.

35.   Lai, S. C. S.; Koper, M. T. M. *Faraday Disc.* **2008,** 140, 399-416.

36.   Colmati, F.; Tremiliosi-Filho, G.; Gonzalex, E. R.; Berna, A.; Herrero, E.; Feliu, J. M. *Faraday Disc.* **2008,** 140, 379-397.

37.   Katsounaros, I.; Schneider, W. B.; Meier, J. C.; Benedikt, U.; Biedermann, P. U.; Cuesta, A.; Auer, A. A.; Mayrhofer, K. J. J. *Physical chemistry chemical physics : PCCP* **2013,** 15, 8058-8068.

38.   Guillaume, P. L. A.; Honoré, K. K.; Albert, T.; Lassiné; Ouattara. *Int. J. Pure Appl. Sci. Technol* **2013,** 14, 33-43.

39.   Chusuei, C. C.; Lai, X.; Luo, K.; Goodman, D. W. *Topics in Catalysis* **2001,** 14, (1-4), 71-83.

40.   Kitsudo, Y.; Iwamoto, A.; Matsumoto, H.; Mitsuhara, K.; Nishimura, T.; Takizawa, M.; Akita, T.; Maeda, Y.; Kido, Y. *Surf. Sci.* **2009,** 603, 2108-2114.

41.   Kuhrt, C.; Harsdorff, M. *Surface Science* **1991,** 245, 173-179.

42.   Wertheim, G. K.; DiCenzo, S. B.; Youngquist, S. E. *Phys. Rev. Lett.* **1983,** 51, (25), 2310-2313.
43.   Kaden, W. E.; Wu, T.; Kunkel, W. A.; Anderson, S. L. *Science* **2009,** 326, 826-9.
44.   Wu, T.; Kaden, W. E.; Kunkel, W. A.; Anderson, S. L. *Surface Science* **2009,** 603, (17), 2764-2770.
45.   Moulder, J. F.; Stickle, W. F.; Sobol, P. E.; Bomben, K. D.; J. Chastain & R. C. King, J., eds., *Handbook of X-ray Photoelectron Spectroscopy*. Physical Electronics: Eden Prarie, MN, 1995.
46.   Wagner, C. D.; Naumkin, A. V.; Kraut-Vass, A.; Allison, J. W.; Powell, C. J.; Jr., J. R. R. *NIST Standard Reference Database 20, Version 3.2 (Web Version)* **2000**.
47.   Xu, Y.; Shelton, W. A.; Schneider, W. F. *Journal of Physical Chemistry A* **2006,** 110, (17), 5839-5846.
48.   Trevor, D. J.; Cox, D. M.; Kaldor, A. *Journal of the American Chemical Society* **1990,** 112, 3742-49.
49.   Taylor, S.; Lemire, G. W.; Hamrick, Y. M.; Fu, Z.; Morse, M. D. *Journal of Chemical Physics* **1988,** 89, 5517-5523.
50.   Kadioglu, Y.; Demirkiran, A.; Yaraneri, H.; Uzengi Akturk, O. *Journal of Alloys and Compounds* **2014,** 591, 188-200.
51.   Nie, A.; Wu, J.; Zhou, C.; Yao, S.; Luo, C.; Forrey, R. C.; Cheng, H. *Int. J. Quantum Chem.* **2007,** 107, 219-224.
52.   Pontius, N.; Bechthold, P. S.; Neeb, M.; Eberhardt, W. *J. Elec. Spectrosc. Rel. Phenom.* **2000,** 106, 107-116.
53.   Ervin, K. M.; Ho, J.; Lineberger, W. C. *Journal of Chemical Physics* **1988,** 89, 4514-21.
54.   Ho, J.; Polak, M. L.; Ervin, K. M.; Lineberger, W. C. *Journal of Chemical Physics* **1993,** 99, 8542-8551.
55.   Achatz, U.; Berg, C.; Joos, S.; Fox, B. S.; Beyer, M. K.; Niedner-Schatteburg, G.; Bondybey, V. E. *Chemical Physics Letters* **2000,** 320, (1,2), 53-58.
56.   Kummerloewe, G.; Balteanu, I.; Sun, Z.; Balaj, O. P.; Bondybey, V. E.; Beyer, M. K. *International Journal of Mass Spectrometry* **2006,** 254, (3), 183-188.
57.   Adlhart, C.; Uggerud, E. *Chem. Comm.* **2006**, 2581-2.
58.   Balteanu, I.; Balaj, O. P.; Beyer, M. K.; Bondybey, V. E. *Phys. Chem. Chem. Phys.* **2004,** 6, 2910-2913.
59.   Hintz, P. A.; Ervin, K. M. *Journal of Chemical Physics* **1995,** 103, 7897-7906.
60.   Yamamoto, H.; Miyajima, K.; Yasuike, T.; Mafune, F. *Journal of Physical Chemistry A* **2013,** 117, (47), 12175-12183.
61.   Kane, M. D.; Roberts, F. S.; Anderson, S. L. *Faraday Disc.* **2013,** 162, 323 - 340.
62.   Kane, M. D.; Roberts, F. S.; Anderson, S. L. *International Journal of Mass Spectrometry* **2014,** 370, 1-15.